

Contents lists available at ScienceDirect

# Heliyon

journal homepage: www.cell.com/heliyon



# Research article

# Unsteady magneto porous convective transport by micropolar binary fluid due to inclined plate: An inclusive analogy

Md. Mosharrof Hossain<sup>a</sup>, R. Nasrin<sup>a,\*</sup>, Md. Hasanuzzaman<sup>b</sup>

### ARTICLE INFO

# Keywords: Magnetohydrodynamics Inclined plate Micropolar fluid Heat and mass transmission Viscous dissipation

# ABSTRACT

In this investigation, the consequence of viscous dissipation on the unstable magneto porous convective transport by a micropolar binary fluid due to an inclined surface with viscous dissipation and thermal radiation is examined. Viscous dissipation plays a noteworthy role in industrial applications. The governing PDEs are converted to combined ODEs with the Boussinesq approximation using a similarity analysis. The obtained non-linear ODEs are resolved using the shooting method with "ODE45 MATLAB" coding assistance. The numerical outcomes are revealed graphically for various dimensionless parameters and numbers, including temperature, concentration, velocity, and micro-rotation. The temperature, micro-rotation, and velocity fields escalate with increasing Eckert numbers. The radiation parameter and variable viscosity parameter increase the flow rate of the fluid. Increasing radiation parameters, suction parameters, and Prandtl numbers lessen the fluid temperature. The buoyancy parameters have symmetrical impacts on the velocity and microrotation of fluid particles in the cooling and heating modes. Improving Eckert number, inclined angle, Schmidt number, Prandtl number, and magnetic parameter reduces skin friction. The heat transmission rate escalates in quantity due to larger Prandtl number values. Rising Prandtl, Eckert, and Schmidt numbers accelerate the mass transfer rate. The current research result is compared to previously published article's result with good agreement.

# 1. Introduction

Everything with weight and space is considered to be matter. Solid, liquid, and gas are the three states of matter. Any substance with the ability to flow can be deemed to be fluid. It can alternatively be narrated as a material that constantly deforms in the presence of shear stress. Both liquid and gas are regarded to be fluids. In fluid dynamics, fluid flow is characterized by several forms, such as laminar, turbulence, compressible and incompressible. The terms non-Newtonian and Newtonian fluids refer to two different categories of fluids. In industrial engineering processes, some non-Newtonian fluids usually flow over vertical surfaces. Notable examples of such fluids are animal blood, paints, fossil fuels, pulps, oil, lubricating greases, honey, molten polymers, etc. They are sometimes used in industrial production. Scholars of fluid dynamics have already studied these non-Newtonian fluid's movement passing vertical and horizontal surfaces. The boundary layer flow is significant for continuously moving surfaces in industrial and engineering applications. Astarita and Marrucci [1] and Bhome [2] examined the characteristics of non-Newtonian fluids in unstable and stable flow states. Alam et al. [3] looked at the steady magnetohydrodynamics boundary layer movement and the united heat and mass transport

E-mail addresses: 0421094019@math.buet.ac.bd (Md.M. Hossain), rehena@math.buet.ac.bd (R. Nasrin), hasanuzzaman@math.kuet.ac.bd (Md. Hasanuzzaman).

https://doi.org/10.1016/j.heliyon.2024.e24314

Received 14 May 2023; Received in revised form 24 October 2023; Accepted 6 January 2024 Available online 9 January 2024

2405-8440/© 2024 The Authors. Published by Elsevier Ltd. This is an open access article under the CC BY-NC-ND license (http://creativecommons.org/licenses/by-nc-nd/4.0/).

<sup>&</sup>lt;sup>a</sup> Department of Mathematics, Bangladesh University of Engineering & Technology, Dhaka, 1000, Bangladesh

<sup>&</sup>lt;sup>b</sup> Department of Mathematics, Khulna University of Engineering & Technology, Khulna, 9203, Bangladesh

<sup>\*</sup> Corresponding author.

#### Nomenclature uniform magnetic field, Am<sup>-1</sup> В suction parameter С fluid concentration, $kg \ m^{-3}$ C $C_f$ local skin friction coefficient specific heat at constant pressure, J kg-1 K-1 $C_p$ $C_s$ concentration susceptibility, m<sup>3</sup>kg<sup>-1</sup> $C_w$ wall concentration, kg m free stream concentration, kg $\,\mathrm{m}^{-3}$ $C_{\infty}$ mass diffusivity coefficient, m<sup>2</sup> s<sup>-1</sup> $D_m$ Ес Eckert number dimensionless velocity f acceleration due to gravity, ms<sup>-2</sup> g Gc solutal Grashof number Gr thermal Grashof number J density of current, Am<sup>-2</sup> thermal conductivity, m<sup>2</sup> s<sup>-1</sup> ĸ $K_r$ chemical reaction parameter thermal diffusion ratio $k_T$ Μ magnetic parameter MHD magnetohydrodynamics Nusselt number $N_u$ Prandtl number $P_r$ radiative heat flux, wm<sup>-2</sup> $q_r$ thermal radiation parameter R Sc Schmidt number Time, s t Т temperature of fluid, K $T_m$ fluid mean temperature, K $T_{w}$ wall temperature, K free stream temperature, K $T_{\infty}$ velocity component along the x-axis, $ms^{-1}$ и uniform surface velocity, $ms^{-1}$ $U_0(t)$ velocity component along the y-axis, ms<sup>-1</sup> β volumetric expansion coefficient with temperature, K<sup>-1</sup> $\beta^*$ volumetric expansion coefficient with concentration, K<sup>-1</sup> similarity variable η dimensionless temperature θ thermophoretic parameter λ kinematic viscosity, m<sup>2</sup> s<sup>-1</sup> fluid density, kg m<sup>-3</sup> ρ similarity parameter $\sigma$ vortex viscosity, Ns/m2 τ ξ Variable viscosity parameter dimensionless concentration ω

through an inclined stretched surface of a non-Newtonian fluid. They discovered that the magnetic parameter causes a drop in the fluid speed, leading to a decrease in mass diffusion and heat convection. A branch of fluid dynamics named magnetohydrodynamics (MHD) studies how a magnetic field causes a fluid that conducts electricity to move. Saltwater, plasmas, electrolytes, and liquid metals are examples of magnetofluids. Both geophysics and engineering benefit from its application. Rahman and Sattar [4] numerically investigated a micropolar fluid's heat transmission and MHD convective fluid movement. In the context of heat absorption or generation with fixed suction, they investigated the fluid movement across a vertical permeable plate moving constantly. They addressed the consequences of the pertinent parameters about the Nusselt number, skin friction, and heat transmission rate. By developing a finite element model, the impacts of homogeneous chemical reaction, viscous dissipation, and Hall current on MHD micropolar fluid on a vertical permeable plate have been explored by Sheri and Shamshuddin [5]. They concluded that the thickness of the thermal boundary layer slowed down as radiation absorption, viscous dissipation, and thermal radiation parameters increased. In contrast, heat absorption and Prandtl number caused it to speed up. The influence of viscous dissipation and thermal radiation on the unstable MHD boundary layer flow of an incompressible fluid across a vertical surface was investigated by Falodun and Fadugba [6]. They

noticed thermal radiation accelerated the convection flow and the fluid's boundary layer.

To characterize the microstructures of materials, porosity is a significant parameter. A solid or group of solid bodies with enough free space within or around them for fluid to pass is known as a porous medium. Kim [7] looked into the unstable 2D laminar flow of an electrically conducting polar fluid with a transverse magnetic field through a semi-infinite vertical porous moving plate. It was assumed that the longitudinal velocity of the plate was constant and that the small perturbation law for free stream velocity was either growing or falling exponentially. In his research, Mohamed [8] looked at the impact of thermal radiation, homogeneous chemical reaction of 1st order, thermal diffusion, and heat source on the unsteady MHD fluid motion across a vertical permeable plate, including suction or mass blowing. The plate had been expected to move at a fixed speed in the flow route with a transverse magnetic field and embedded in a homogenous porous medium. The rotational influences on unstable MHD binary diffusive flow passing an impulsively initiated vertical permeable surface through varying mass diffusion and temperature with thermal radiation were considered by Sharma et al. [9]. It was observed that the temperature field tends to rise when the Prandtl number and radiation parameter decline. Arshad et al. [10] observed the viscous fluid boundary layer flow across a permeable, flat surface with heat and mass transport using various study parameters. The fluid motion was detected to rise when the viscoelastic parameter, permeable medium parameter, and unsteadiness parameter improved. According to Eringen [11], micropolar fluid is any fluid created from spherical particles or randomly oriented with specific micro-rotations. Physical examples of intrinsically polarized micropolar fluids include blood flows, ferrofluids, liquid crystals, bubbly liquids, etc. Shamshuddin and Thumma [12] developed a mathematical model over a porous media for the heat and mass transport from an inclined surface. They also involved a heat source or sink, including incompressible, dissipative, magnetohydrodynamic, and chemically reactive micropolar fluid flow. Guedri et al. [13] deliberated an incompressible, steady 2D stream of micropolar fluid upon an extensible sheet. The concentration distribution exhibited declining behavior when the Brownian motion number was enhanced. In contrast, Ali et al. [14] investigated axisymmetric slip flow past a bullet-shaped object exponentially stretching. According to the experiment, stretching an object with a bullet shape caused a higher heat transmission rate than whenever the object was stable. Hossain et al. [15] explored a numerical examination of unstable convective thermal and mass transportation over a vertical permeable plate along with chemical reaction, thermophoresis, radiative thermal transfer, and uniform magnetic field. They revealed that the temperature-dependent dynamic viscosity significantly enhanced the fluid velocity and reduced the particle's micro-rotation near the wall.

Heat and mass transmission are the fundamental science for many industrial processes, and technical and scientific devices. Heat and mass transmission procedures are vital in numerous industries, including aerospace, automotive, power generation, materials processing, chemical processing, industrial equipment, and rotating machinery. Murthy et al. [16] discovered how thermal radiation and Hall current affected a natural convection heat and mass transmission flow crossing a vertical permeable plate in an unstable MHD model. They thought the plate was embedded in a similar porous material and oscillated constantly with a transverse magnetic field.

Hamid et al. [17] looked at the aspects of heat transmission and the influences of chemical reactions on time-dependent Williamson fluid flow across a linear stretching surface. They concluded that temperature and thermal boundary layer thickness reduced the Prandtl number functions. Babar [18] studied MHD unsteady heat and mass transmission through a vertical permeable plate on the free convection micropolar fluid movement with radiation and chemical reaction. They found that increasing the Schmidt, Soret, and Dufour numbers reduced the concentration outlines when considering the chemical reaction parameter. Raju et al. [19] explored the influences of combined convection with chemical reaction and thermal radiation on the MHD flow of incompressible, electrically conducting, viscous fluid upon a continuously inclined warm porous surface. They perceived that the temperature distribution was reduced when the radiation and heat source parameters increased. Dawar et al. [20] investigated the heat and mass transmission properties of two-dimensional [2D] micropolar fluid movement with chemical reactions stimulated by thermophoresis, magnetic field, Brownian motion, Joule heating, and magnetic field. They observed that the velocity distribution improved as the material parameter rose, but an adverse effect was seen on the micro-rotational distribution. Hossain et al. [21] discussed the impact of thermal radiation on the motion of a micropolar binary fluid mixture on a continuously permeable surface during unstable magnetic convection heat and mass transmission. When fluid is in motion, specific amounts of the kinetic energy are converted into thermal energy by the fluid. The fluid viscosity converts specific amounts of kinetic energy into thermal energy. Viscous dispersion is the term used to describe irreversible processes caused by viscosity. Similar to an energy source, which significantly impacts heat transfer rates, viscous dissipation is essential in changing the temperature distribution.

The Eckert number is typically used to describe the influences of viscous dissipation, which are significant in geophysical movements and some industrial applications. The influences of thermo-diffusion and diffusion-thermo through free convective heat and mass transmission of an electrically conducting fluid over a permeable medium were observed by Eldabe et al. [22]. The numerical findings showed that the velocity dropped as the non-Newtonian and magnetic parameters enhanced. Mostafa et al. [23] considered how a non-Newtonian fluid passing a vertically extended surface was affected by the joint impacts of radiation and viscous dissipation. This study stated that the wall temperature of the fluids could be raised by using a powerful magnetic field. For a time-dependent Williamson fluid flow caused by a permeable stretching/shrinking sheet, Hamid et al. [24] revealed the combined impacts of a magnetic field, Ohmic heating, and viscous dissipation for a Williamson fluid flow that is time-dependent. They were caused by a permeable stretching/shrinking sheet. It was discovered that dual solutions are limited to a particular range of shrinking parameters, while the stretching situation had only one solution. Dharmaiah et al. [25] investigated the influence of heat source, thermophoresis, and Hall current over a dissipative-adjusted MHD combined convection stream surrounding an inclined surface placed in a porous medium. Through an inclined permeable surface in a conducting field, they considered a double diffusion fluid in addition to a chemical reaction and a heat source. The consequences of a heat source, a chemical reaction, and an aligned magnetic parameter were all observed to significantly impact the velocity distribution and the behaviors of the profiles. Rajakumar et al. [26] discussed the effects of chemical reaction and viscosity dissipation on unsteady MHD free convective flow across a continuous vertical porous plate with radiation absorption. Pandikunta et al. [27] looked at the impact of thermal radiation and viscous dissipation on an unstable MHD

micropolar fluid flow through a vertical porous plate, including the variation of wall heat. They observed that microparticles in the fluid caused it to absorb more heat, increasing the fluid temperature through viscous dissipation and heat generation. Fenuga et al. [28] considered the impact of the Eckert number and radiation parameter over an MHD flow with a heat transmission rate close to a stagnation point. Eckert number and radiation caused a lessening heat transmission rate at the surface. As radiation increased, flow temperature further improved for velocity ratio parameters. Ferdows et al. [29] outlined the parameterized action of free convection micropolar fluid across a horizontally stretched sheet by dynamic behavior comprising thermal diffusion, viscous dissipation, and diffusion-thermo. The findings demonstrated that the vortex viscosity ratio, suction, and radiation parameters all caused a reduction in the micropolar fluid velocity. The impacts of viscous dissipation and radiative on unstable magneto-conductive heat-mass transport over a vertical permeable surface were investigated by Hasanuzzaman et al. [30]. It had been found that higher Eckert numbers, radiative parameters, and local Grashof numbers all resulted in higher fluid velocity.

Earlier, the researchers played a significant role in studying the dynamic behavior comprising thermal diffusion, viscous dissipation, diffusion-thermo, and radiative on unstable magneto-conductive heat-mass transmission upon a vertical permeable sheet. In previous research, the authors observed the numerical investigation of unstable convective heat and mass transmission flow on a vertical permeable plate. We take the initiative to extend the above research work for an inclined porous surface to study three positions (horizontal, vertical, and inclined surfaces) of the porous plate at a time to compare the results with published papers. Through the research, we intend to consider a continuous permeable surface for more investigations about the properties of fluid flow of the micropolar binary fluid.

Motivated by the above research studies, we discuss an unsteady magneto porous convective transport by a micropolar binary fluid due to an inclined plate with viscous dissipation and thermal radiation. In this investigation, we thoroughly investigate fluid particle's temperature, velocity, microrotation, and concentration characteristics to perceive the influences of selected parameters or numbers. To further elucidate the innermost feature of the fluid movement, the thermo-physical extents of practical implication, such as the surface couple stress, Sherwood number, Nusselt number, and skin friction, are revealed in tabular forms.

# 2. Mathematical analysis

We consider a micropolar binary fluid crossing a moving porous plate for time-dependent magneto-convective heat and mass transmission. Fig. 1 displays the physical model. Here, flow is determined along the x-axis. It must also be in an infinite space with the y-axis perpendicular to it. An optically thin fluid satisfies the condition  $\alpha \ll 1$ , where  $\alpha$  denotes the absorption coefficient. The term  $\frac{\partial q_r}{\partial y}$  is known as the radiative heat flux, which is the fourth power of temperature in the energy balance equation, as Cheng [31]. We assume the temperature gradient  $\left(\frac{\partial T}{\partial y}\right)$  across the surface as well as the temperature gradient  $\left(\frac{\partial T}{\partial y}\right)$  perpendicular to the surface in the theory of boundary layer as  $\frac{\partial T}{\partial y} \gg \frac{\partial T}{\partial x}$ . We choose to satisfy the condition  $T_w < T_\infty$ , where  $T_w$  and  $T_\infty$  represent wall temperature and free stream temperature, respectively. Furthermore, magnetic Reynolds is taken as small due to ignorance of the induced magnetic field. We also discard the electric field and the Hall effect of MHDs.

According to Sastry et al. [32] and Animasaun [33], the mathematical model to describe the governing equations along with Boussinesq's approximation and the stated assumptions is as follows:

$$\frac{\partial v}{\partial y} = 0 \tag{1}$$

$$\frac{\partial u}{\partial t} + v \frac{\partial u}{\partial y} = \left(\frac{\mu + \tau}{\rho}\right) \frac{\partial^2 u}{\partial y^2} + \frac{\tau}{\rho} \frac{\partial N}{\partial y} + g\beta(T - T_{\infty})\cos\gamma + g\beta^*(C - C_{\infty})\cos\gamma - \frac{\sigma B_0^2}{\rho} u \tag{2}$$

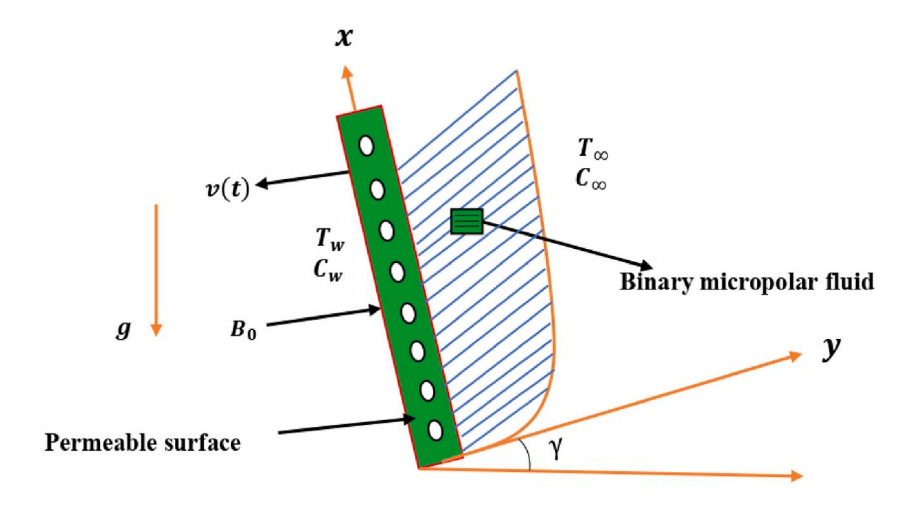


Fig. 1. Coordinate system [2D] along with physical model.

$$\rho C_p \left( \frac{\partial T}{\partial t} + v \frac{\partial T}{\partial v} \right) = \kappa \frac{\partial^2 T}{\partial v^2} - \frac{\partial q_r}{\partial v} + \nu \left( \frac{\partial u}{\partial v} \right)^2 \tag{3}$$

$$\frac{\partial C}{\partial t} + v \frac{\partial C}{\partial v} + \frac{\partial}{\partial v} [V_T(C - C_\infty)] = D_m \frac{\partial^2 C}{\partial v^2}$$
(4)

$$\frac{\partial N}{\partial t} + v \frac{\partial N}{\partial y} = \frac{\gamma^*}{\rho j} \frac{\partial^2 N}{\partial y^2} - \frac{\tau}{\rho j} \left( 2N + \frac{\partial u}{\partial y} \right) \tag{5}$$

Here  $B_0$  denotes a uniform transverse magnetic field that acts over y-axis. The quantity  $\nu$  can be regarded as either a constant or a function of t by doing with equation (1) in this situation. Along y-axis, the velocity component is given by Makinde [34] as follows –

$$v = -c\left(\frac{\nu}{t}\right)^{1/2} \tag{6}$$

where the injection and suction parameters are denoted by c < 0 and c > 0, respectively. In the following way, Rahman [35] and Qasim and Sheltie [36] established the concepts of microinertia per mass and spin gradient viscosity:

$$\gamma^* = \left(\mu + \frac{\tau}{2}\right)j,\tag{7}$$

where  $j = \frac{\mu}{\rho U_0}$ .

Talbot et al. [37] initiated the thermophoretic parameter provided by the equation (4). Afterwards, Tsai et al. [38] introduced the said parameter as given below:

$$V_T = -\frac{K^{Th}}{T_{ref}} \frac{\partial T}{\partial y} \tag{8}$$

where  $K^{Th}$  is the thermophoretic coefficient. The values of  $K^{Th}$  were taken from 0.2 to 1.2 by Batchelor and Shen [39]. Joseph Boussinesq proposed buoyancy-driven flow back in 1903. He looked at density variations corresponding to buoyancy-driven flow and acceleration caused by gravity. Considering the change of least temperature between the free stream layer and wall, density model is-

$$\rho = \rho_{\infty} [1 - \beta (T - T_{\infty})] \tag{9}$$

The buoyancy term is expressed as  $g(\rho - \rho_{\infty})$  and hence given by-

$$g(\rho - \rho_{\infty}) = -g\beta\rho_{\infty} (T - T_{\infty}) \tag{10}$$

We define the pressure term (buoyancy force) by  $-\frac{\partial p}{\partial x} = g\beta \rho_{\infty} (T - T_{\infty})$ . Also, the following formula can be set to describe the Boussinesq approximation for heat and mass transfer:

$$-\frac{\partial p}{\partial x} = g\beta \rho_{\infty} (T - T_{\infty}) + g\beta^{*} \rho_{\infty} (C - C_{\infty})$$
(11)

This assumption is called the Boussinesq approximation. Even when they come in the form of multiplication by g, Boussinesq [40] claimed that density differences are extremely minor to be omitted, where g indicates the gravitational acceleration.

Then, Boussinesq approximation (11) is modified as:

$$-\frac{\partial p}{\partial x} = g\beta \rho_{\infty}(T_{\infty} - T) + g\beta^{*}\rho_{\infty}(C_{\infty} - C)$$
(12)

Mukhopadhyay [41] created the model of temperature-dependent viscosity. It was earlier discussed by Batchelor [42]. The equation  $\mu(T) = \mu^*[1 + b(T_w - T)]$  was produced by Animasaun and Anselm [43] which satisfies the condition  $T_w > T_\infty$ . Another form of this equation is given by-

$$\mu(T) = \mu^* [1 + b(T_{\infty} - T)] \tag{13}$$

This is correct for  $T_w < T_\infty$ .

The term  $q_r$  denotes the radiative heat flux which is described by Raptis [44] as presented below-

$$q_r = -\frac{4\sigma^*}{3k^*} \cdot \frac{\partial T^4}{\partial v} \tag{14}$$

The Stefan-Boltzmann constant is indicated here by the symbol  $\sigma^*$  whereas the mean absorption coefficient by  $k^*$ . Raptis [45] assumed the changes in temperature as tiny in the flow. The flow of fluids can therefore be expressed by means of a linear temperature function. Neglecting the terms of higher order and expanding  $T^4$  in a Taylor series about  $T_0$ , we have

$$T^4 \cong 4T_0^3 T - 3T_0^4 \tag{15}$$

with the help of the relations [12,13], equation [2] becomes-

$$\frac{\partial u}{\partial t} + v \frac{\partial u}{\partial y} = \frac{1}{\rho} \frac{\partial}{\partial y} \left( \mu \frac{\partial u}{\partial y} \right) + \frac{\tau}{\rho} \frac{\partial^2 u}{\partial y^2} + \frac{\tau}{\rho} \frac{\partial N}{\partial y} + g\beta(T_{\infty} - T)\cos\gamma + g\beta^*(C_{\infty} - C)\cos\gamma - \frac{\sigma B_0^2}{\rho} u$$
(16)

then equation [3] implies that,

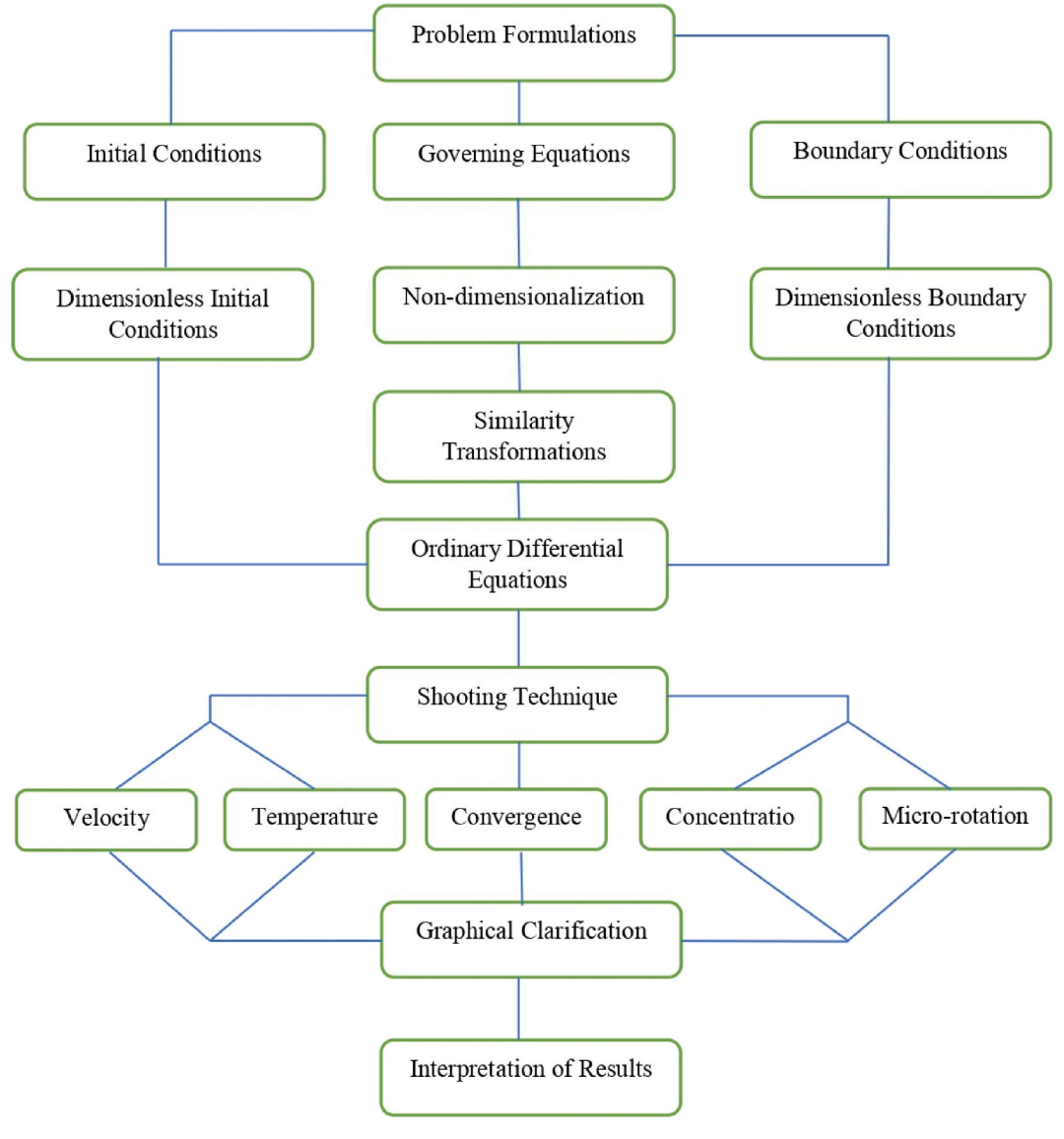
$$\rho C_p \left( \frac{\partial T}{\partial t} + \nu \frac{\partial T}{\partial y} \right) = \kappa \frac{\partial^2 T}{\partial y^2} - \frac{\partial q_r}{\partial y} + \nu \left( \frac{\partial u}{\partial y} \right)^2 \tag{17}$$

Using the equation [12], equation [4] becomes-

$$\frac{\partial C}{\partial t} + v \frac{\partial C}{\partial y} + \frac{\partial}{\partial y} \left[ V_T(C_\infty - C) \right] = D_m \frac{\partial^2 C}{\partial y^2}$$
(18)

The equation [5] can be written following equation [7] as-

$$\frac{\partial N}{\partial t} + v \frac{\partial N}{\partial y} = \left[ \frac{\mu(T)}{\rho} + \frac{\tau}{2\rho} \right] \frac{\partial^2 N}{\partial y^2} - \frac{\tau U_0}{\mu(T)} \left( 2N + \frac{\partial u}{\partial y} \right) \tag{19}$$



Flowchart as well as solution framework.

The equations [16–19] are subjected to the boundary conditions [20–22] according to Animasaun [33]:

$$u(y,0) = 0, T(y,0) = T_w, N(y,0) = 0, C(y,0) = C_w \text{ for } t \le 0$$
 (20)

$$u(0,t) = 0, \ T(0,t) = T_w, \ N(0,t) = m_0 \frac{\partial u}{\partial t}, \ C(0,t) = C_w \ for \ t > 0$$
 (21)

$$u(\infty, t) \to U_0, \ T(\infty, t) \to T_m, \ N(\infty, t) \to 0, \ C(\infty, t) \to C_m \ for \ t > 0$$
 (22)

The boundary conditions mentioned above satisfy the conditions  $C_w < C_\infty$  and  $T_w < T_\infty$ . From the equation [21], no-spin condition is derived as N(0, t) = 0, where  $m_0 = 0$ .

We introduce the following dimensionless variables into [16–19]:

$$\eta = \frac{y}{2\sqrt{\nu t}} \; ; \quad f(\eta) = \frac{u}{U_0} \; ; \; \theta(\eta) = \frac{T}{T_{\infty}} \; ; \; \varphi(\eta) = \frac{C}{C_{\infty}} \; ; \; h(\eta) = \frac{N\sqrt{\nu t}}{U_0}$$
 (23)

Finally, the resulting dimensionless non-linear ODEs are obtained as:

$$(1 + \xi - \theta \xi + k_1)f' - \xi \theta' f' + 2(\eta + c)f' + 2k_1h' + G_r\xi(1 - \theta)\cos\gamma + G_c\xi(1 - \varphi)\cos\gamma - Mf = 0$$
(24)

$$\theta' + \frac{Pr}{1+R} \left\{ 2 (\eta + c)\theta' + Ec f'^2 \right\} = 0$$
 (25)

$$\varphi'' + 2S_c(\eta + c)\varphi' - \lambda S_c(1 - \varphi)\theta' + \lambda S_c\theta'\varphi' = 0$$
(26)

$$\left(1 + \xi - \theta \xi + \frac{k_1}{2}\right)h' + 2(\eta + c)h' + 2h - \frac{8L_1}{1 + \xi - \theta \xi}h - \frac{2L_1}{1 + \xi - \theta \xi}f' = 0$$
(27)

The temperature, velocity, and concentration functions converge to 1, while the micro-rotation function converges to 0 as the similarity variable is taken outside the boundary. With regard to the aforementioned problem, the dimensionless boundary conditions are:

$$f(\eta) = 0, \theta(\eta) = \theta_w, h(\eta) = -\frac{1}{4}f'(0), \varphi(\eta) = \varphi_w \text{ at } \eta = 0$$
 (28)

$$f(\eta) \to 1, \theta(\eta) \to 1, h(\eta) \to 0, \varphi(\eta) \to 1 \text{ as } \eta \to \infty$$
 (29)

where the dimensionless quantities/parameters/numbers are as follows:

 $\eta$  is a similarity variable,

 $\theta(\eta)$  denotes temperature function,

 $f(\eta)$  denotes velocity function,

 $h(\eta)$  denotes micro-rotation function,

 $\varphi$  ( $\eta$ ) denotes concentration function,

 $G_r = \frac{4tg\beta}{U_0h}$  is identified as thermal Grashof number,

 $k_1 = \frac{\tau}{\mu}$  is known as micro-rotation,  $\xi = bT_{\infty}$  is identified as variable viscosity,  $G_c = \frac{4tg\beta^s}{U_0b}$  is identified as solutal Grashof number,  $R = 4t\frac{4\sigma\alpha^2T_{\infty}^2}{\rho C_pT_{\infty}}$  is the radiation,  $Pr = \frac{\nu}{\gamma} = \frac{\mu C_p}{\kappa}$  is the Prandtl number,  $\omega = \frac{E_A}{T_{\infty}R_G}$  is the activation energy,  $L_1 = k_1U_0t$  is identified as time dependent micro-rotation,  $\lambda = -\frac{\kappa^{ThT_{\infty}}}{\nu T_{pef}}$  is identified as thermophoresis,

 $Sc = \frac{\nu}{D_m}$  is identified as Schmidt number,

 $M = \frac{4\sigma B_0^2 L_1}{\rho k_1 U_0}$  is identified as magnetic field,

 $\gamma$  is identified as an angle of inclination, and

 $E_c = \frac{U_0^2}{T_{\rm m}\rho C\rho}$  is known as Eckert number.

### 3. Method of solution

This research work presents an investigation of the impact of viscous dissipation on unstable magneto porous convective transference by micropolar binary fluid due to an inclined plate with thermal radiation. The first step is to use modified Boussinesq's approximation to convert the higher order non-linear PDEs [1–5] into second order simultaneous ODEs. With the help of the similarity technique, it is again transformed into an initial value problem described by Ali et al. [46,47] and Uddin and Nasrin [48]. Using numerical methods, we successfully solve coupled non-linear ODEs [24–27] with boundary conditions [28,29] applying the shooting technique.

# 3.1. Numerical results

The non-dimensional temperature, velocity, microrotation, and concentration fields are computed contrary to the dimensionless coordinate  $\eta$  with the previously described numerical technique, with modifications in several thermophysical quantities dominating the fluid flow phenomenon. Figs. 2–12 exhibit the numerical findings of the problem. For studying the inner features of the fluid

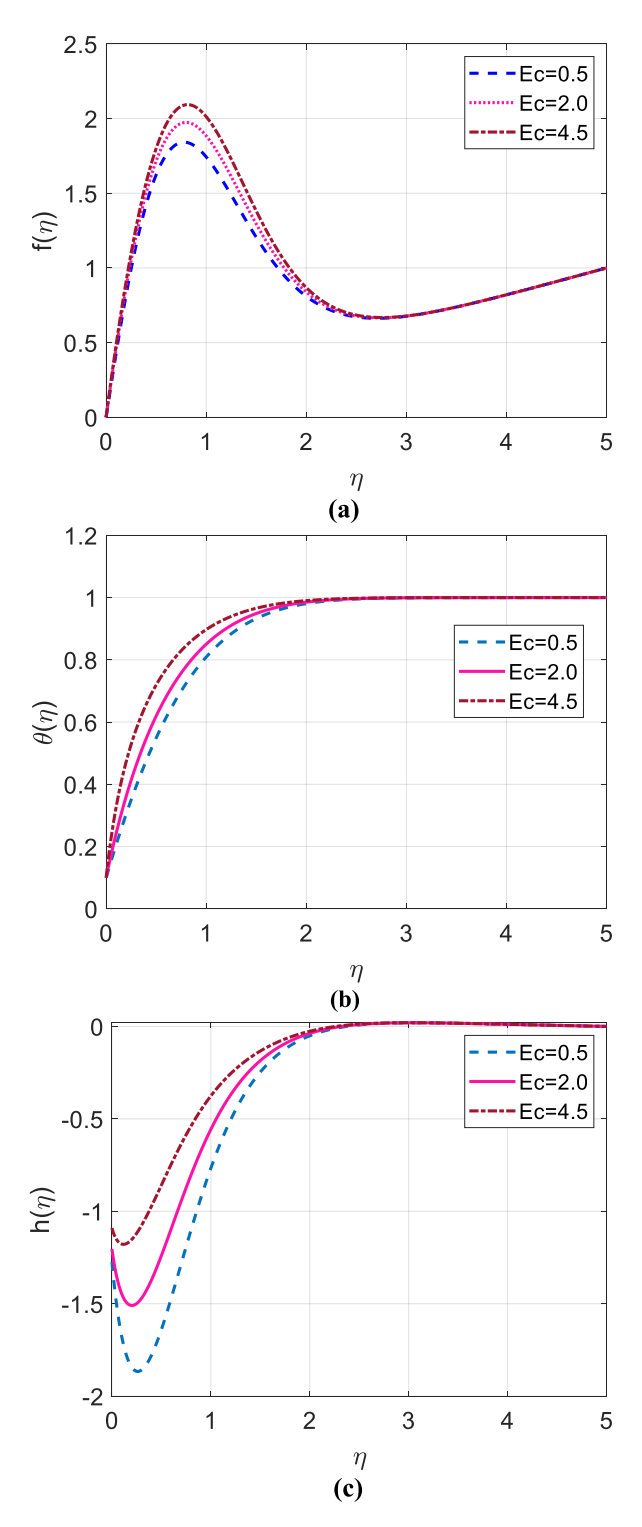


Fig. 2. Profiles of (a) velocity, (b) temperature, and (c) micro-rotation for a few Eckert number disparity.

motion, the thermo-physical values of hands-on use, such as Nusselt number, surface couple stress, skin friction coefficient, and Sherwood number are additionally determined and shown in Tables 1–6. Tables 7–10 compare the numerical outcomes of the current findings with a published work. The parameters or, numbers are listed as: Prandtl number (Pr), Eckert number (Ec), thermal Grashof number (Gr), temperature dependent variable viscosity ( $\xi$ ), an inclined angle ( $\gamma$ ), magnetic field (M), solutal Grashof number (Gc), thermal radiation (R), thermophoresis ( $\lambda$ ), micro-rotation ( $K_1$ ), Schmidt number (Sc), suction parameter (c), and time dependent micro-rotation ( $L_1$ ). For further elaboration and accurate investigation, this study's physical parameters are precisely selected. The ranges of these parameters are Ec (0.5-4.5),  $\gamma$  ( $0^0-180^0$ ), M(1-5), Pr (0.63-1), Sc (0.16-0.3), R (0-1.5), c (0.1-2),  $\lambda$  (1-8),  $\xi$  (1-2.5), Gr (1-15-15). It is stated that just the changing of one selected parameter or number is made while looking at the influence of that parameter or number on the field variables. The remaining of the numbers or parameters have been treated as fixed. We use parameters or numbers having specific values as: Ec = 2, Pr = 0.71, R = 0.5,  $\gamma = 45^\circ$ , Gc = 10,  $L_1 = 0.33$ ,  $\lambda = 1$ , Sc = 0.22, c = 0.5,  $\xi = 3$ , Gr = 10,  $K_1 = 0.5$  and M = 2. Also, at a finite point of  $\eta = 5$ , the boundary conditions at infinity are implemented.

# 3.1.1. Effect of Eckert number

Fig. 2(a-c) are used to illustrate how Eckert number (*Ec*) affects the profiles of temperature, velocity, and micro-rotation. It is believed that an upsurge of *Ec* makes velocity to increase, which is shown in Fig. 2(a). Physically, growing velocity is caused by an increase in the magnitude of *Ec*, because it represents the relationship between the enthalpy difference in kinetic energy and boundary layer. Developing Eckert number values correspond to more significant velocity gradients in the boundary layer. Therefore, due to improved friction in the area, more heat is produced near the surface, and due to the higher kinetic energy of the molecules, the velocity rises. Fig. 2(b) is the variation in temperature concerning *Ec*. We apply *Ec* to show the impact of self-heating of fluid due to dissipation effects. We perceive from the Figure that inner friction between high-speed fluid layers also influences the flow

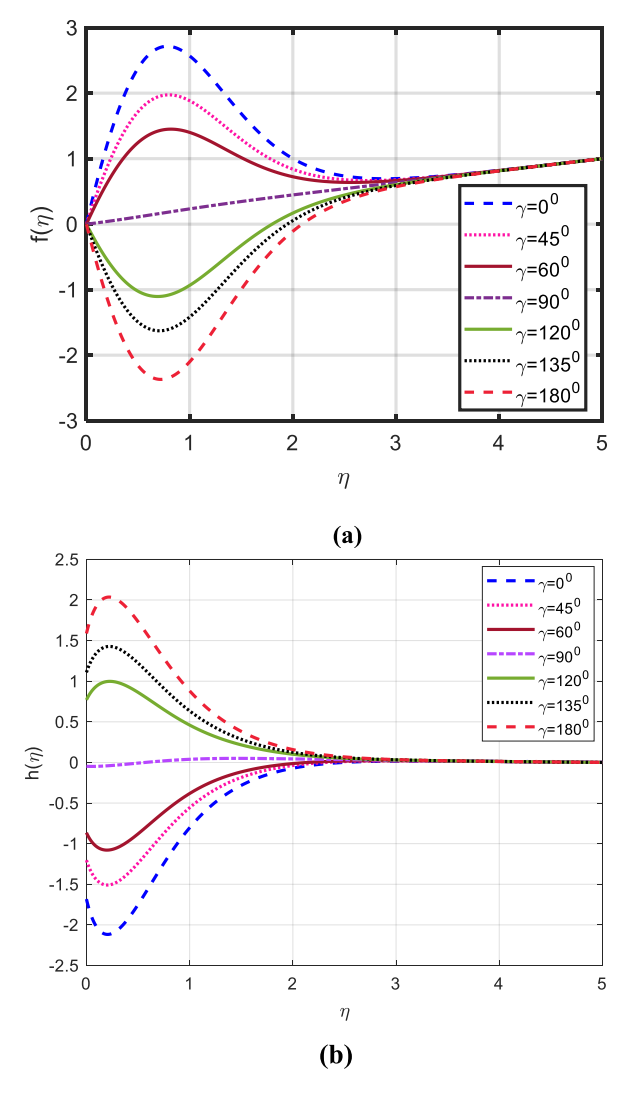


Fig. 3. Profiles of (a) velocity and (b) micro-rotation for inclined angle disparity.

temperature. When the *Ec* comes up, it is detected that the temperature further improves. Fig. 2(c) shows that with an escalation in *Ec*, the micro-rotation field improves.

# 3.1.2. Effect of inclination

Fig. 3(a-b) demonstrate the effect of inclined angle ( $\gamma$ ) on the profiles of micro-rotation and velocity. We notice that the velocity tends to decline at increasing levels of gamma. Because of the multiplication factor  $\cos \gamma$ , the resultant effect of the buoyant force diminishes for increasing amounts of  $\gamma$ , and as a result, the velocity rapidly falls for growing values of  $\gamma$ . It is additionally noted that fluid velocity is a strictly monotonic rising function for horizontal position ( $\gamma = 90^{\circ}$ ). Nevertheless, the higher gamma values indicate an opposite tendency, as shown in Fig. 3(b). This results from the fact that inclination angle rises within the boundary layer, angular momentum does as well. The micro-rotation profile is improved as a result.

# 3.1.3. Effect of magnetic field

The influence of the magnetic field upon translational and angular velocity is shown in Fig. 4(a–b). With one exception, the magnetic field's effect is opposite of the fluid's material characteristics since the magnetic field creates a resistive electromagnetic force (Lorentz force), and the translational velocity drops. Fig. 4(b) reveals that angular velocity is improved everywhere by a rise in magnetic field intensity. The buoyancy force, heat source, and viscous dissipation all interacted to increase the speed, which can be attributed to the resistive force.

# 3.1.4. Effect of Prandtl number

Fig. 5(a–c) demonstrate the Prandtl number (*Pr*) behavior over the micro-rotation, velocity, and temperature profiles. The viscosity is discovered to be proportional to the Prandtl number. For growing amounts of *Pr*, the kinematic viscosity rises as well. In turn, this

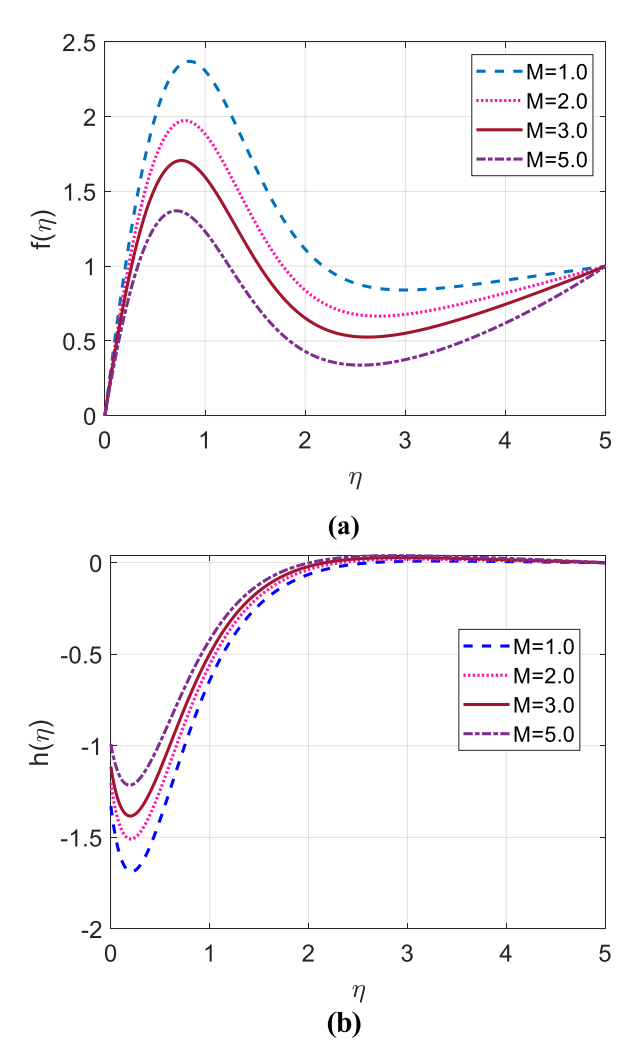


Fig. 4. Profiles of (a) velocity and (b) micro-rotation for magnetic field disparity.

causes the fluid to get thicker and slow down. The Prandtl number for oxygen is 0.63, gas is 0.71, and steam is 1. From Fig. 5(a), it is remarkable that fluid's viscosity accelerates with rising values of Pr. As a result, the fluid particles are unable to flow easily. Consequently, the fluid speed diminishes. As Pr increases, the temperature reduces, as seen in Fig. 5(b). Physically, higher Prandtl numbers have comparatively low heat conductivity. Consequently, heat conduction is declined, which causes a drop in temperature. Because of this, when Pr increases, heat transmission rate rises and hence the temperature profile lessens. However, the micro-rotation profiles exhibit adverse effects when Pr is improved. It is discovered that the micro-rotation profiles significantly rise close to the surface  $0 \le \eta \le 2.2$  and further than this tends to zero as  $\eta \to 5$ .

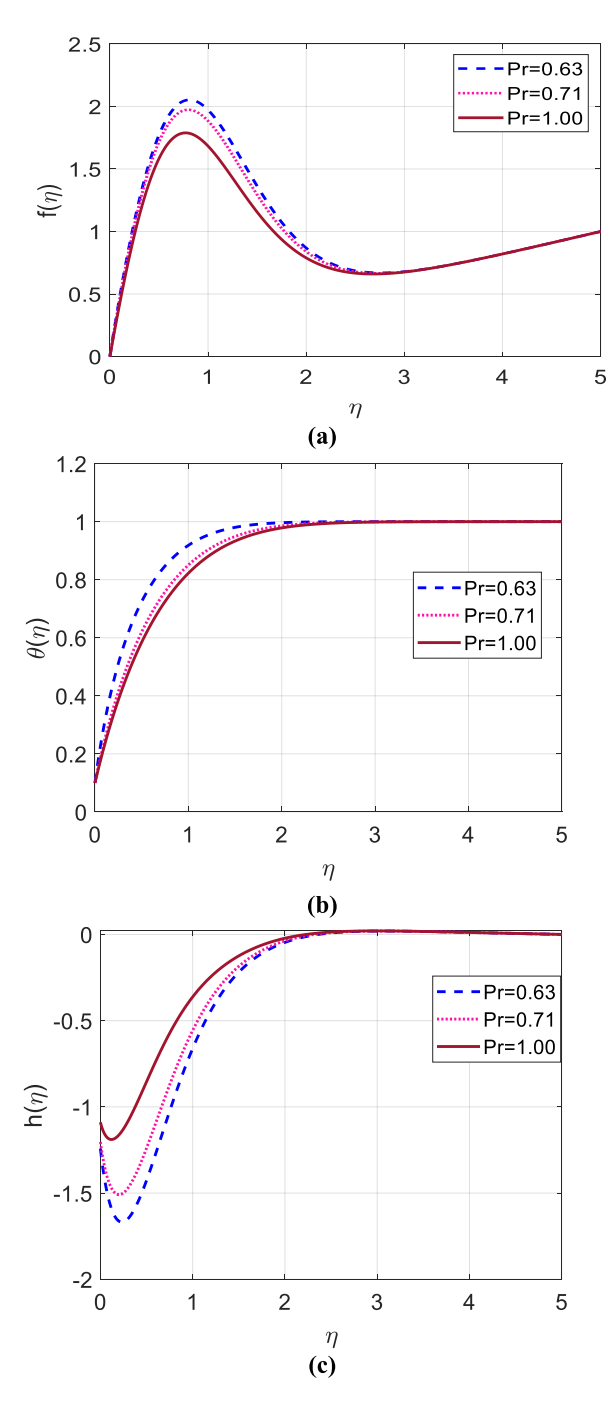
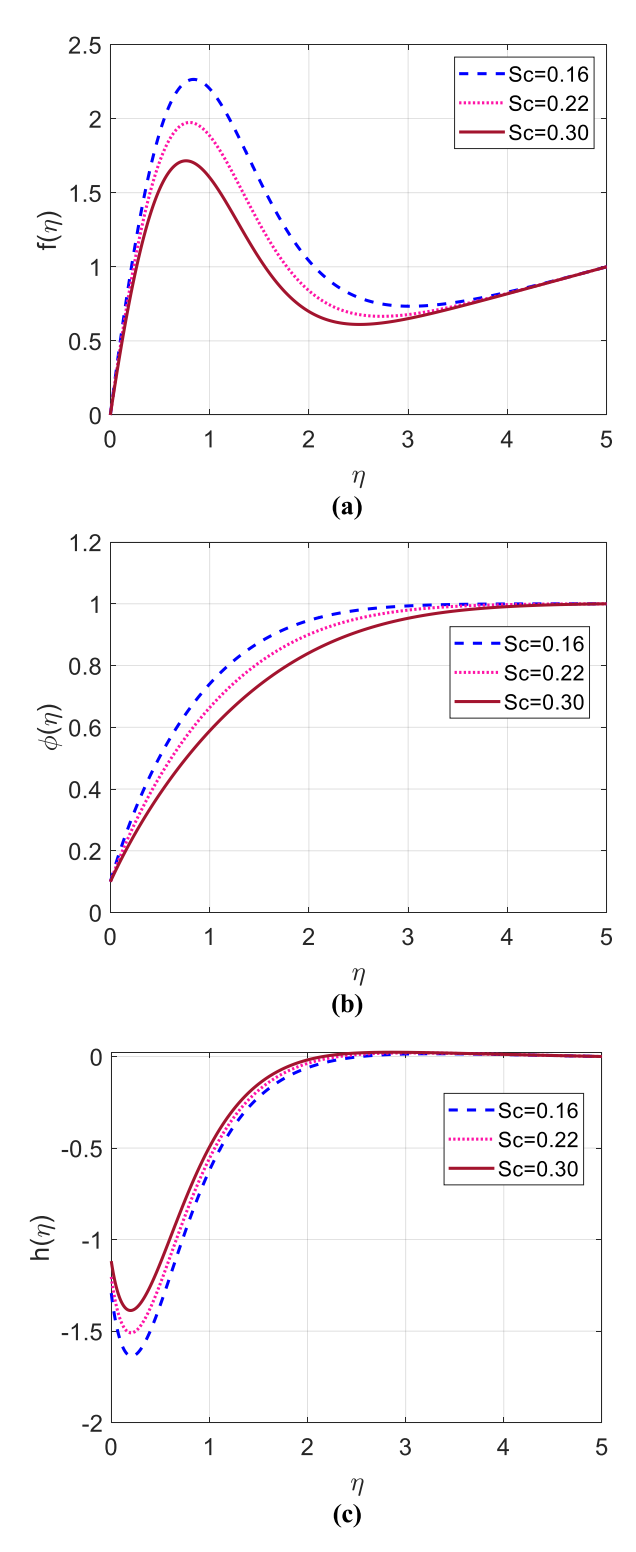


Fig. 5. Profiles of (a) velocity, (b) temperature, and (c) micro-rotation for Prandtl number disparity.



 $\textbf{Fig. 6.} \ \ \text{Profiles of (a) velocity, (b) temperature, and (c) micro-rotation for Schmidt number disparity.}$ 

# 3.1.5. Effect of Schmidt number

Fig. 6(a-c) present the impacts of Schmidt number (Sc) on the concentration, velocity, and micro-rotation outlines. It is evident that molecular diffusivity is found to be inversely proportional to Sc. The density and momentum level losses identical thickness and diffusivity rates when Sc = 1. The momentum propagation rate surpasses the species propagation rate when Sc is more significant

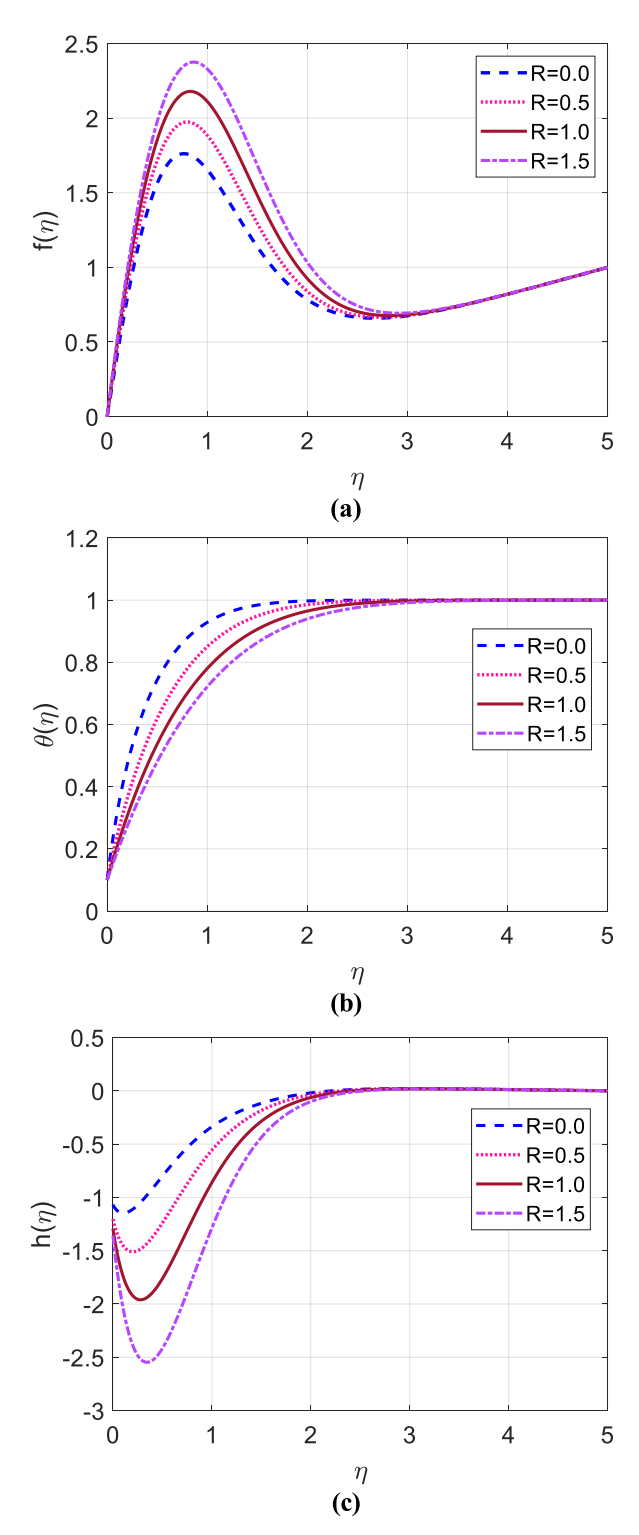


Fig. 7. Profiles of (a) velocity, (b) temperature, and (c) micro-rotation for radiation disparity.

(Sc > 1). Additionally, the Schmidt number and kinematic viscosity (v) inversely correlated. Nevertheless, an adverse effect is noticed in Fig. 6(a), fluid's kinematic viscosity rises as the Schmidt number does. As a result, the fluid particles unable to continue freely. Therefore, the fluid's speed declines. The impact of several amounts of Sc on the concentration profile is shown in Fig. 6(b). For increasing levels of Sc, it is discovered that the profile of concentration declines. Because of the consequent reduction in mass

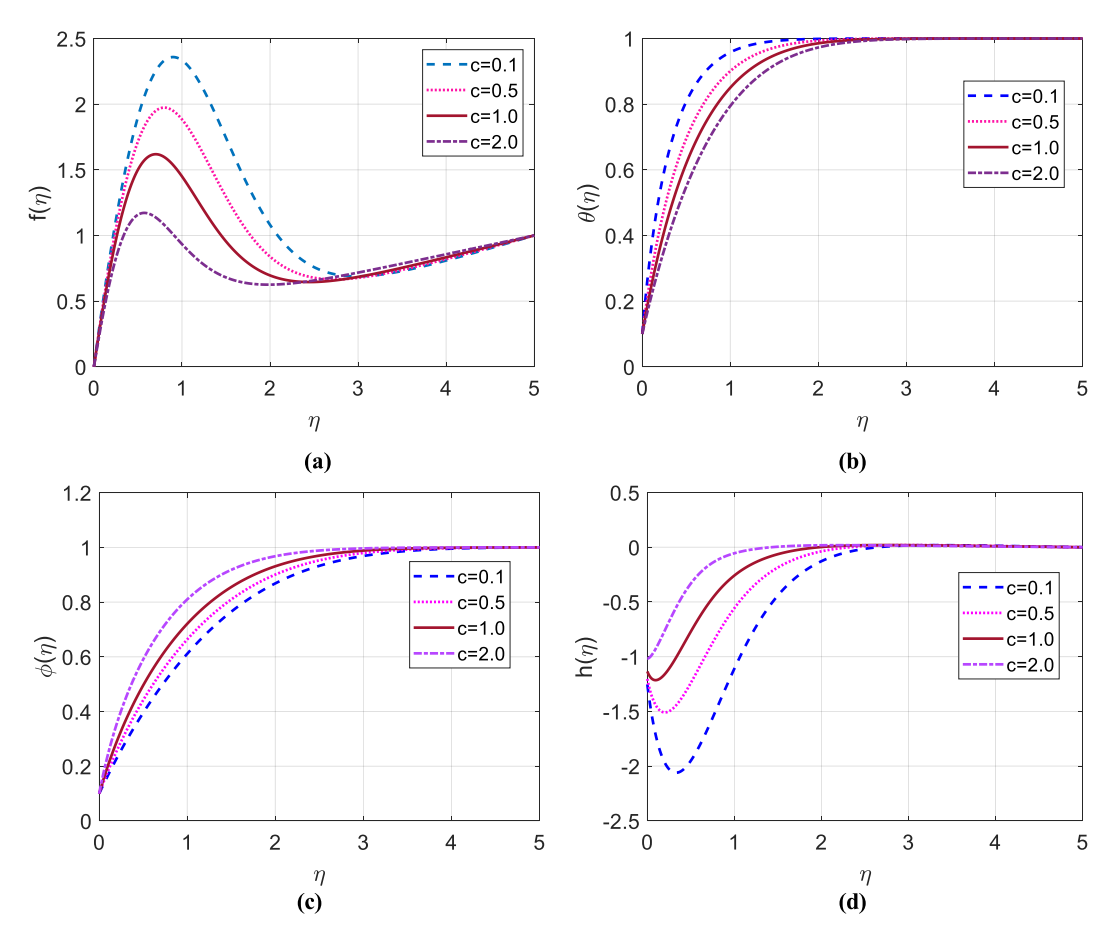


Fig. 8. Profiles of (a) velocity, (b) temperature, (c) concentration, and (d) micro-rotation for suction disparity.

diffusivity, concentration levels are reduced through less intense mass transmission. Consequently, concentration boundary layer thickness diminishes. This results from the interaction between mass transfer and velocity field, and the Schmidt number can be used to influence the species distribution in materials. In Fig. 6(c), the properties of Sc on the micro-rotation fields are depicted. As expected, the micro-rotation profiles relative to the wall  $0 \le \eta \le 2.6$  significantly increase with Sc increasing. After that, there is no noticeable change in the behavior, and it eventually approaches zero asymptotically.

### 3.1.6. Effect of thermal radiation

The impressions of the thermal radiation parameter (R) on the profiles of temperature, velocity, and micro-rotation are revealed in Fig. 7(a-c). Rising values of R increase temperature, because the ratio of conduction heat transmission to thermal radiation transmission represents the radiation parameter. The outcome is an escalation in speed and a reduction in fluid viscosity within the boundary layer. In contrast, this demonstrates that the thermal boundary layer thickens whenever radiation is present because radiation provides an extra channel for energy dissipation. Consequently, the temperature drops as the amounts of R enhance. Additionally, we perceive that the temperature upsurges when the radiation parameter is set to higher values with  $\eta$ . The micro-rotation fields reduce with increasing R in the range of  $0 \le \eta \le 2.6$ , and following that, there is no longer an effect seen with growing  $\eta$ , and they asymptotically approach zero as  $\eta \to 5$ .

# 3.1.7. Effect of suction

Fig. 8(a-d) show the properties of the suction parameter (c) on the fields of micro-rotation, velocity, species concentration, and temperature. Greater values of c correlate with a lessening in fluid motion from the wall to the free stream, as would be predicted. Because the low momentum fluid surrounding the warm wall is removed by suction. Separation and transition are consequently deferred. The fluid near the warm wall is forced toward the area where buoyancy forces due to the significant effect of viscosity slow down its movement. We also note that fluid motion started to grow with  $\eta$  and reached its most significant peak within  $0.5 \le \eta \le 1$  and after that typically approaches one asymptotically as  $\eta \to 5$ .

With variations in c, Fig. 8(b) demonstrates the manner in which the temperature profile fluctuates. With rising levels of c, it appears that temperature lowers. This results from the boundary layer flow zone being cooled by the suction. According to Fig. 8(c), the species concentration across the boundary layer improved together with the amounts of c. The thinner boundary layer traveling

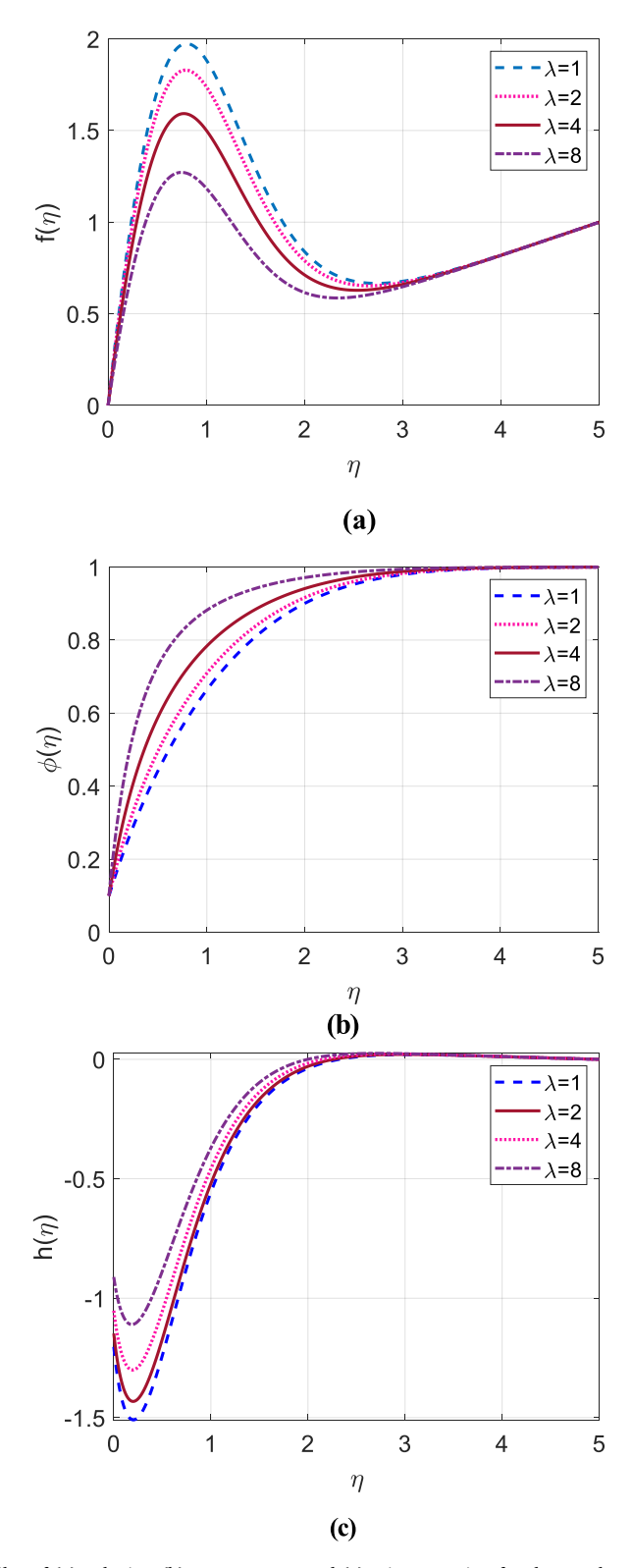


Fig. 9. Profiles of (a) velocity, (b) temperature, and (c) micro-rotation for thermophoresis disparity.

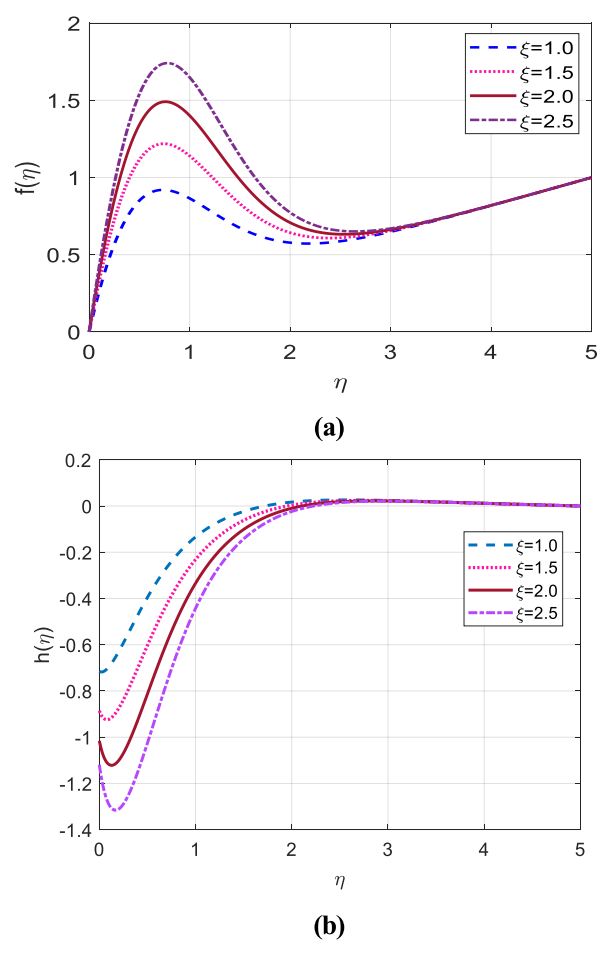


Fig. 10. Profiles of (a) velocity and (b) micro-rotation for viscosity disparity.

over the inclined porous surface will be eliminated as the species advances from a lower concentration to a greater concentration owing to a rise in suction. The effect is that the high-density fluid will quickly concentrate towards the surface. We further mark that the micro-rotation field escalates with a growth in suction, where  $0 \le \eta \le 2.6$ . After that  $(2.6 \le \eta \le 5)$ , the rising value of c does not affect the micro-rotation profiles.

# 3.2. Effect of thermophoresis

Fig. 9(a-c) display the micro-rotation, concentration, and velocity outlines for several amounts of thermophoretic parameter  $(\lambda)$ . We know that the transport force that happens as a result of a temperature gradient is called thermophoresis. Physically, higher values of thermophoretic parameters reduce the thickness of the momentum boundary layer, and hence, the velocity declines. As  $\lambda$  increases, the concentration and microrotation fields exhibit the opposite behavior. A tiny change to the thermophoresis parameter causes a sharp increase in fluid velocity. Due to the surplus heat energy produced, the concentration distribution rapidly expands. We also discover that the micro-rotation field close to the wall  $(0 \le \eta \le 2.2)$  is significantly impacted by an upsurge in  $\lambda$ . After that, the micro-rotation field has no more impact as  $\lambda$  and typically approaches zero asymptotically as  $\eta \to 5$ .

# 3.2.1. Effect of variable viscosity

The micro-rotation and velocity distributions for numerous amounts of viscosity parameter ( $\xi$ ) are revealed in Fig. 10(a-b). The velocity field near the wall ( $0 \le \eta \le 3$ ) is growing well and thereafter no effect is observed and at last tends to 1 asymptotically as  $\eta \to 5$ . This is because the fluid's intermolecular force weakens as it warms, causing the molecules to become agitated and start moving. As  $\xi$  rises, improvements are made in the speed from the wall to the free stream. because the energy of this movement causes the fluid's viscosity to decrease as it moves away from the wall gradually. Fig. 10(b) displays that the growing amount of  $\xi$  causes a considerable diminution in micro-rotation fields close to the wall. This finding suggests that the micro-rotation of particles adjacent to the wall reduces when vortex viscosity depends on temperature constantly, because the fluid therein is more viscous. After that, there is no longer any effect, and finally, as  $\eta$  approaches 5, the micro-rotation tends to zero.

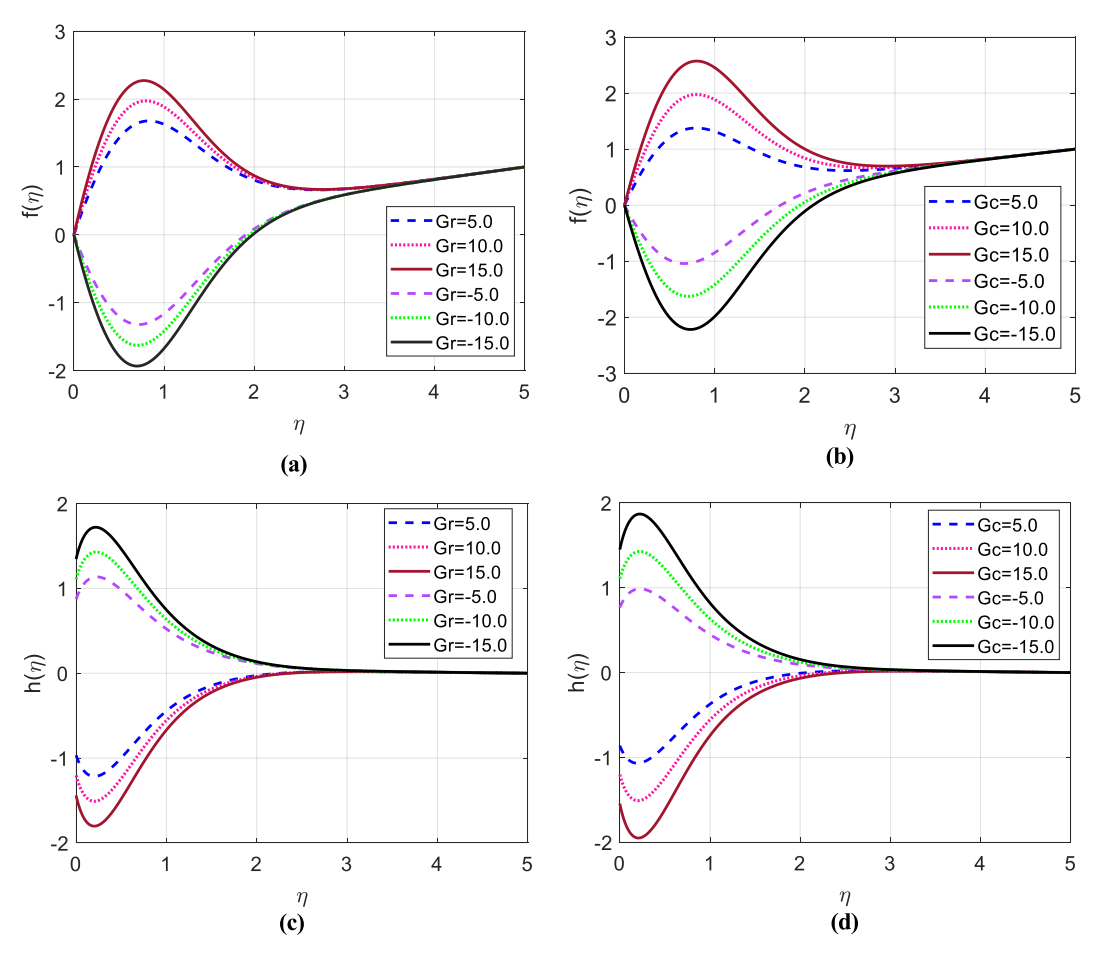


Fig. 11. Profiles of (a) and (b) velocity, (c) and (d) micro-rotation for thermal Grashof number and solutal Grashof number variation, respectively.

# 3.2.2. Effect of thermal and solutal Grashof numbers

The features of solutal Grashof number (Gc) and thermal Grashof number (Gr) on the profiles of micro-rotation and velocity are displayed in Fig. 11(a–d). Fig. 11(a–b) illustrate how thermal and solutal Grashof numbers have the same influence on velocity. We discover that acceleration improves with larger values of Gr and Gc. This is because the Grashof number roughly expresses the ratio of buoyancy to viscous forces acting on a fluid. However, there is a slight difference in the highest value of  $f(\eta)$ , which at  $\eta=0.8$  is determined to be 2.25 for Gr and 2.5 for Gc. It is widely known that enhancing the buoyancy parameters (Gr and Gc) will improve fluid motion. Furthermore, it is clear from both the figures that neither Gr nor Gc has an impact when the fluid is away from the wall where  $3.2 < \eta < 5$ .

Fig. 11(c–d) show the exact effects of local solutal and thermal Grashof numbers on the microrotation fields. As they improve from zero to positive quantities, the microrotation field weakens from the opposing side that is near the wall, where  $0 \le \eta \le 2.6$ . The microrotation fields are then completely unaffected by Gr and Gc and asymptotically approach Gc approach Gc and Gc are the microrotation field rises from the positive side near the wall as above. Following this, it is discovered that Gc and Gc have the same effects on the microrotation fields.

# 3.2.3. Effect of time

The influences of time (t) on the profiles of micro-rotation and velocity are discovered in Fig. 12(a–b). It is well known that time is proportional to thermal radiation, and the ratio of conduction heat transmission to thermal radiation transmission refers to the radiation parameter. The result is an escalation in fluid velocity and a reduction in fluid viscosity within the boundary layer. In contrast, this demonstrates that the thermal boundary layer thickens whenever radiation is present because radiation provides an extra channel for energy dissipation. Consequently, the temperature drops as the values of thermal radiation enhance. So, growing values of t increase the fluid velocity. But the micro-rotation fields lessen with rising amounts of t in the range of  $0 \le \eta \le 2$ , and after then, nothing is observed as  $\eta$  is elevated and finally, they asymptotically approach zero as  $\eta \to 5$ .

## 3.2.4. Skin friction, Nusselt number, Sherwood number, and surface couple stress

To clarify the inner functioning of the fluid motion, the thermo-physical parameters of practical significance are also tabulated.

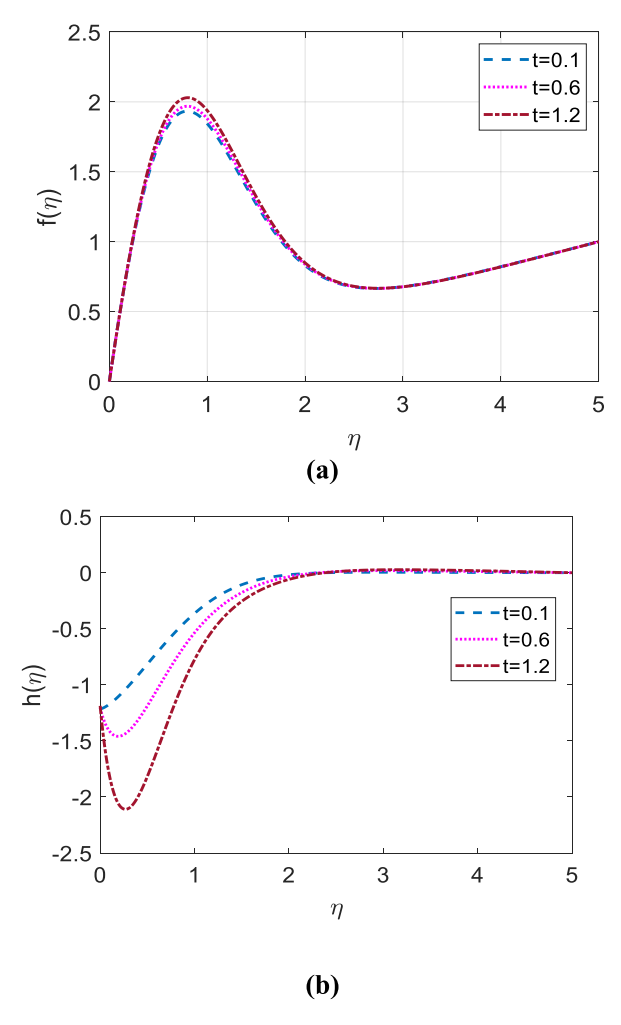


Fig. 12. Profiles of (a) velocity and (b) micro-rotation for time disparity.

Table 1 Impact of Prandtl number on thermo-physical quantities  $(C_f, N_u, S_h, C_s)$ .

Pr	f(0)	$-\stackrel{'}{ heta'}(0)$	$-arphi^{'}(0)$	h'(0)
0.71	4.81410410344806	1.56385772859692	0.877283425554583	-3.97335758558069
1.00	4.35732606260281	2.40907939872377	1.03882062974159	-2.16367012098834

Table 2 Impact of thermal Grashof number on thermo-physical quantities  $(C_f, N_u, S_h, C_s)$ .

Gr	f'(0)	$-\stackrel{'}{ heta'}(0)$	-arphi'(0)	h'(0)
5	3.8676795872763	1.56385772859692	0.87728342555458	-3.2170221893176
10	4.8141041034480	1.56385772859692	0.87728342555458	-3.9733575855806
15	5.7605286196271	1.56385772859692	0.87728342555458	-4.7296929817531
-5	-3.4881395281022	1.56385772859692	0.87728342555458	3.0897558625731
-10	-4.4345640442776	1.56385772859692	0.87728342555458	3.8460912585025
-15	-5.3809885604535	1.56385772859692	0.87728342555458	4.6024266547807

The properties of thermal Grashof number (Gr) on Sherwood number  $(S_h)$ , Nusselt number  $(N_u)$ , skin-friction  $(C_f)$ , and surface couple stress  $(C_s)$  are presented in Table 2. In the presence of heating (Gr < 0) and cooling (Gr > 0),  $C_f$  is seen to fall and grow, respectively, although  $C_s$  exhibits the opposite trend. In both circumstances (Gr > 0) and Gr < 0, it is further noticeable that Gr has impact neither on  $N_u$  nor on  $S_h$ . Additionally, it is discovered that as Gr improves from 5 to 15,  $C_f$  enhances by approximately 49 % while  $C_s$  declines by about 47 %.

Table 3 Impact of Eckert number on thermo-physical quantities (Cf,  $N_{tt}$ ,  $S_h$ ,  $C_s$ ).

Ec	$f^{'}(0)$	$-\stackrel{.}{ heta'}(0)$	$-arphi^{'}(0)$	h'(0)
0.5	5.09224887050167	1.10438924486964	0.790069415139180	-5.87545921287564
2	4.81410410344806	1.56385772859692	0.877283425554583	-3.97335758558069
4.5	4.36210802572650	3.00013899711185	1.15578405935799	-1.97654724253684

Table 4 Impact of magnetic field on thermo-physical quantities  $(C_f, N_u, S_h, C_s)$ .

М	$\dot{f}(0)$	$-\stackrel{.}{ heta'}(0)$	$-  \varphi^{'}(0)$	$h^{'}(0)$
1	5.3194574590670	1.56385772859692	0.87728342555458	-4.5069352746880
2	4.8141041034480	1.56385772859692	0.87728342555458	-3.9733575855806
3	4.4540161834382	1.56385772859692	0.87728342555458	-3.5985890636045
4	4.1812165455289	1.56385772859692	0.87728342555458	-3.3185353881854

**Table 5** Impact of inclined angle on thermo-physical quantities  $(C_i, N_u, S_h, C_s)$ .

γ	$\dot{f}(0)$	$-\stackrel{'}{ heta'}(0)$	$-ec{arphi'}(0)$	$h^{'}(0)$
0	6.72957321881919	1.56385772859705	0.877283425554683	-5.59282457323569
45	4.81406486462851	1.56385772859705	0.877283425554683	-3.97332441043130
60	3.45967162412927	1.56385772859705	0.877283425554683	-2.82822886990286
90	0.18977002951343	1.56385772859705	0.877283425554683	-0.06363316735554
120	-3.08013156497906	1.56385772859705	0.877283425554683	2.70096254322242
135	-4.43452480546896	1.56385772859705	0.877283425554683	3.84605808335614
180	-6.35003315879207	1.56385772859705	0.877283425554683	5.46555825881172

**Table 6** Impact of Schmidt number on thermo-physical quantities (Cf,  $N_{lo}$ ,  $S_{lo}$ , Cs).

Sc	f(0)	$-\stackrel{'}{ heta'}(0)$	$-arphi^{'}(0)$	$h^{'}(0)$
0.16	5.16941162672397	1.56385772859692	0.699511215918274	-4.3592007775591
0.22	4.81410410344806	1.56385772859692	0.877283425554583	-3.9733575855806
0.3	4.46984625784297	1.56385772859692	1.10231051938734	-3.6042420622941

Table 7 For several Schmidt number values, comparison of local heat transmission rate  $-\vec{\theta}(0)$ .

Values of Sc	$-\theta'(0)$ Animasaun [33]	$-\stackrel{'}{ heta(0)}$ Present study	Percentage of error
Sc = 0.22 $Sc = 0.42$	1.267068597902801 1.280521268663868	1.2997337198343 1.2997337250693	3 % 2 %
Sc = 0.62	1.287403287660129	1.2997337295552	1 %

These parameters are Nusselt number ( $N_u$ ), surface couple stress ( $C_s$ ), Sherwood number ( $S_h$ ), and skin friction ( $C_f$ ), which correspond to  $\theta'(0)$ , h'(0),  $\varphi'(0)$ , and f'(0), respectively. We have used parameters or numbers with specific values as: Ec=2,  $\gamma=5^\circ$ ,  $\xi=3$ ,  $K_1=0.5$ ,  $L_1=1.33$ , R=0.5, M=2, P=0.71,  $\lambda=1$ , M=10, M=10, M=10, and M=10 are several values of one selected number or parameter to observe the influence on the physical parameters. As mentioned above, the remaining parameters/numbers are chosen with fixed values.

Table 1 exhibits the impact of various Prandtl number (Pr) values on Sherwood number  $(S_h)$ , surface couple stress  $(C_s)$ , skin-friction  $(C_f)$ , and Nusselt number  $(N_u)$ . Here,  $C_f$  is just one thermo-physical quantity that reduces with rising Pr values, although all other quantities  $C_s$ ,  $S_h$ ,  $N_u$  enhance. For rising amounts of Pr (0.71-1),  $C_f$  falls by approximately 10 %. But as Pr is improving (0.71-1), so  $C_s$ ,  $S_h$ ,  $N_u$  are all raised by approximately 46 %, 17 %, and 54 %, respectively.

The consequences of Eckert number (Ec) on Sherwood number ( $S_h$ ), Nusselt number ( $N_u$ ), skin-friction ( $C_f$ ), and surface couple stress ( $C_s$ ) are revealed in Table 3. Now, we notice that the thermo-physical parameters ( $N_{tb}$ )  $S_h$ ,  $C_s$ ) improve whereas only  $C_f$  drops with greater amounts of Ec. Furthermore, we observe that for elevating values Ec (0.5–4.5),  $C_f$  reduces by about 14 %. Moreover, all other physical quantities  $N_{tb}$ ,  $S_{tb}$ ,  $C_s$  improve by nearly 173 %, 46 %, and 66 %, respectively, in growth of Ec (0.5–4.5).

Table 4 explains the influences of magnetic parameter (M) on Sherwood number ( $S_h$ ), surface couple stress ( $C_s$ ), skin-friction ( $C_f$ ), and Nusselt number ( $N_u$ ). From this table, we realize that  $C_f$  lessens for growing amounts of M but an opposite behavior is noticed for  $C_s$ . The outcomes of the Table also show that M has impacts neither on  $N_u$  nor on  $S_h$  for higher quantities of M. For improving amounts of M (1–4), the table also demonstrates that  $C_f$  diminishes by around 21 %, whereas  $C_s$  rises by about 27 %.

**Table 8** For several Schmidt number, comparison of local mass transmission rate  $-\varphi'(0)$ .

Values of Sc	$-\varphi'(0)$ Animasaun [33]	-arphi'(0) Present study	Percentage of error
Sc = 0.22	0.798091264284715	0.8248981332868	3 %
Sc = 0.42	1.279330713448670	1.3245705722381	4 %
Sc = 0.62	1.728144872634346	1.7902286400053	6 %

**Table 9** For several suction values, comparison of local heat transmission rate  $-\vec{\theta}(0)$ .

Values of <i>c</i>	$-\stackrel{.}{ heta}(0)$ Animasaun [33]	$-\stackrel{.}{ heta}(0)$ Present study	Percentage of error
c = 0.0	0.83868669297265	0.8557102698422	2 %
c = 0.5	1.23006859790280	1.2997337198343	7 %
c = 1	1.75390102523921	1.8024800834775	5 %
c = 1.5	2.28161487460779	2.3448217644316	6 %

**Table 10** For several suction, comparison of local mass transmission rate  $-\varphi'(0)$ .

Values of c	$-arphi^{'}(0)$	$-arphi^{'}(0)$	Percentage of error
	Animasaun [33]	Present study	
c = 0	0.58272723586718	0.60341674929391	2 %
c = 0.5	0.79809126428471	0.82489813328681	2 %
c = 1	1.03833456571078	1.07126976059664	3 %
c = 1.5	1.29706507428797	1.33570874990471	4 %

The properties of the inclined angle ( $\gamma$ ) on Sherwood number ( $S_h$ ), skin-friction ( $C_f$ ), surface couple stress ( $C_s$ ), and Nusselt number ( $N_u$ ) are revealed in Table 5. It shows that  $C_f$  lessens for rising quantities of  $\gamma$ , although  $C_s$  has the reverse effect. Moreover, for uprising amounts of  $\gamma(0^0 - 180^0)$ , no effect is noticed on  $N_u$  and  $S_h$ . Also, we remark that  $C_f$  weakens by approximately 97 % while  $C_s$  advances by approximately 99 % for the growing quantities of  $\gamma(0^0 - 90^0)$ .

The impacts of Schmidt number (Sc) on Sherwood number ( $S_h$ ), skin-friction ( $C_f$ ) surface couple stress ( $C_s$ ), and Nusselt number ( $N_u$ ), are displayed in Table 6. The figure shows that as the magnitude of Sc grows,  $C_f$  declines while  $S_h$  and  $C_s$  express contrary affects. Furthermore, it is evident that for increasing amounts of Sc, no effect of Sc occurs only on  $N_u$ . We further notice that  $C_f$  declines by around 14 %, whereas  $S_h$  and  $C_s$  promote by about 57 % and 17 %, respectively, in rising of Sc (0.16–0.3).

# 3.2.5. Comparison

The numerical outcomes of the current research work are compared with those of the published paper Animasaun [33] in Tables 7–10. Tables 7 and 8 exhibit the comparison of Nusselt number ( $N_u$ ) and Sherwood number ( $N_u$ ), respectively for several amounts of Schmidt number ( $N_u$ ), whereas Tables 9 and 10 display the comparison of  $N_u$  and  $N_u$ , respectively for several amounts of suction parameter ( $N_u$ ). The comparison appears to bear a good agreement.

### 4. Conclusion

The viscous dissipative impacts on unstable magneto porous convective transference by micropolar binary fluid due to an inclined plate with thermal radiation are studied in this investigation.

We can derive the following conclusions from our numerical results:

- The temperature, velocity, and micro-rotation fields escalate with an Eckert number increase (Ec).
- Higher amounts of Prandtl number (*Pr*), radiation parameter (*R*), and suction parameter (*c*) reduce the temperature of fluid particles.
- With more significant amounts of the thermophoretic parameter (λ) and suction parameter (c), the species concentration upgrades, whereas Schmidt number (Sc) diminishes the fluid concentration.
- The rising amounts of Schmidt number (Sc), inclined angle ( $\gamma$ ), Prandtl number (Pr), magnetic parameter (M), suction parameter (R), and thermophoretic parameter (R) develop the micro-rotation fields. But a reverse impact is noticed for variable viscosity parameter (R).
- For increasing amounts of inclined angle (γ), Prandtl number (*Pr*), suction parameter (c), thermophoretic parameter (λ), Schmidt number (*Sc*), and magnetic parameter (*M*), the velocity decelerates. On the other hand, variable viscosity parameters (ξ) and radiation parameters (*R*) quicken the fluid motion.

• The buoyancy parameters (*Gr* and *Gc*) have symmetrical effects on the velocity as well as microrotation of fluid particles in cases of heating (*Gr* < 0) and cooling (*Gr* > 0).

- Improving values of Prandtl number (0.71–1), Eckert number (0.5–4.5), magnetic force parameter (1-4), inclined angle (0<sup>0</sup> 90<sup>0</sup>), and Schmidt number (0.16–0.3) lessen skin-friction by about 10 %, 14 %, 21 %, 97 %, and 14 %, respectively. But the above physical variable upgrades by about 49 % for rising amounts of thermal Grashof number (5-15)].
- The heat transfer rate escalates in quantity by around 173 % and 54 % due to larger values of thermal Grashof number (5-15) and Prandtl number (0.71–1), respectively.
- Growing amounts of Schmidt number (0.16–0.3), Eckert number (0.5–4.5) and Prandtl number (0.71–1) promote mass transmission rate by around 57 %, 46 % and 17 %, respectively.

#### CRediT authorship contribution statement

**Md. Mosharrof Hossain:** Conceptualization, Formal analysis, Investigation, Methodology, Validation, Writing – original draft. **R. Nasrin:** Conceptualization, Formal analysis, Methodology, Resources, Supervision, Writing – original draft, Writing – review & editing. **Md. Hasanuzzaman:** Conceptualization, Methodology, Validation, Writing – review & editing.

# Declaration of competing interest

The authors would like to confirm that there are no known conflicts of interest associated with this publication and there are no significant financial support for this work that could have influenced its outcome. We confirm that the manuscript has been read and approved by all named authors and that there are no other persons who satisfied the criteria for authorship but are not listed. We further confirm that the order of authors listed in the manuscript has been approved by all of us. We confirm that we have given due consideration to the protection of intellectual property associated with this work and that there are no impediments to publication, including the timing of publication, with respect to intellectual property. In so doing we confirm that we have followed the regulations of our institutions concerning intellectual property. We confirm that we have provided a current, correct email address which is accessible by the Corresponding Author.

# Appendix A. Supplementary data

Supplementary data to this article can be found online at https://doi.org/10.1016/j.heliyon.2024.e24314.

# References

- [1] G. Astarita, G. Marrucci, Principles of Non-newtonian Fluid Mechanics, McGraw-Hill, New York, 1974.
- [2] G. Böhme, Series in Applied Mathematics and Mechanics, North-Holland, 1987.
- [3] M.S. Alam, M.R. Islam, M. Ali, M.A. Alim, M.M. Alam, Magnetohydrodynamic boundary layer flow of non-Newtonian fluid and combined heat and mass transfer about an inclined stretching sheet, Open J. Appl. Sci. 5 (6) (2015) 279–294.
- [4] M.M. Rahman, M.A. Sattar, The magnetohydrodynamic convective flow of a micropolar fluid past a continuously moving vertical porous plate in the presence of heat generation/absorption, ASME Journal Heat Transfer 128 (2) (2005) 142–152.
- [5] S. Sheri, M.D. Shamshuddin, Finite element analysis on transient magnetohydrodynamic (MHD) free convective chemically reacting micropolar fluid flow past a vertical porous plate with Hall current and viscous dissipation, Propulsion and Power Research 7 (4) (2018) 353–365.
- [6] B.O. Falodun, S.E. Fadugba, Effects of heat transfer on unsteady magnetohydrodynamics (MHD) boundary layer flow of an incompressible fluid a moving vertical plate, World Scientific News 88 (2) (2017) 118–137.
- [7] Y.J. Kim, Unsteady MHD convection flow of polar fluids past a vertical moving porous plate in a porous medium, Int. J. Heat Mass Tran. 44 (15) (2001) 2791–2799.
- [8] R.A. Mohamed, Double-diffusive convection-radiation interaction on unsteady MHD flow over a vertical moving porous plate with heat generation and Soret effects, Appl. Math. Sci. 3 (13) (2009) 629–651.
- [9] R.P. Sharma, V. Ravikumar, M.C. Raju, G.S.S. Raju, S.V.K. Varma, Rotational impact on unsteady MHD double diffusive boundary layer flow over an impulsively emerged vertical porous plate, Journal of International Academy of Physical Sciences 20 (4) (2016) 303–317.
- [10] M. Arshad, A. Hussain, A. Hassan, S.A.G.A. Shah, M.A. Elkotb, S. Gouadria, M. Alsehli, A.M. Galal, Heat and mass transfer analysis above an unsteady infinite porous surface with chemical reaction. Case Stud. Therm. Eng. 36 (2022) 102140.
- [11] A.C. Eringen, Theory of micropolar fluids, Journal of Mathematics and Mechanics (1966) 1–18.
- [12] M.D. Shamshuddin, T. Thumma, Numerical study of a dissipative micropolar fluid flow past an inclined porous plate with heat source/sink, Propulsion and Power Research 8 (1) (2019) 56–68.
- [13] K. Guedri, N. Ameer Ahammad, S. Nadeem, E.M. Tag-ElDin, A.U. Awan, M.F. Yassen, Insight into the heat transfer of third-grade micropolar fluid over an exponentially stretched surface, Sci. Rep. 12 (1) (2022) 15577.
- [14] M. Ali, R. Nasrin, M.A. Alim, Axisymmetric boundary layer slip flow with heat transfer over an exponentially stretching bullet-shaped object: a numerical assessment, Heliyon 9 (3) (2023) e13671.
- [15] M. Hossain, M.M.T. Hossain, R. Nasrin, Time-dependent magneto-convective thermal-material transfer by micropolar binary mixture fluid passing a vertical surface, Science & Technology Asia 28 (1) (2023) 33–47.
- [16] M.R. Murthy, R.S. Raju, J.A. Rao, Heat and mass transfer effects on MHD natural convective flow past an infinite vertical porous plate with thermal radiation and Hall current, Procedia Eng. 127 (2015) 1330–1337.
- [17] A. Hamid, M. Khan, M. Alghamdi, Numerical simulation for transient flow of Williamson fluid with multiple slip model in the presence of chemically reacting species, Int. J. Numer. Methods Heat Fluid Flow 29 (11) (2019) 4445–4461.
- [18] R. Biswas, M. Mondal, K. Shanchia, R. Ahmed, S. Samad, S.F. Ahmmed, Explicit finite difference analysis of an unsteady magnetohydrodynamics heat and mass transfer micropolar fluid flow in the presence of radiation and chemical reaction through a vertical porous plate, Journal of Nanofluids 8 (7) (2019) 1583–1591.

[19] M.C. Raju, C. Veeresh, S.V.K. Varma, K.B. Rushi, K.A.G. Vijaya, Heat and mass transfer in MHD mixed convection flow on a moving inclined porous plate, J. Appl. Comput. Math. 4 (5) (2015) 1–7.

- [20] A. Dawar, Z. Shah, A. Tassaddiq, S. Islam, P. Kumam, Joule heating in magnetohydrodynamic micropolar boundary layer flow past a stretching sheet with chemical reaction and microstructural slip, Case Stud. Therm. Eng. 25 (2021) 100870.
- [21] M. Hossain, R. Nasrin, M. Hasanuzzaman, Radiative and MHD effects on time-dependent thermal-material transfer by micropolar binary mixture, Advances in Mathematical Physics 2022 (2022), 2224435, 18.
- [22] N.T. Eldabe, S.N. Sallam, M.Y. Abou-zeid, Numerical study of viscous dissipation effect on free convection heat and mass transfer of MHD non-Newtonian fluid flow through a porous medium, Journal of the Egyptian Mathematical Society 20 (2) (2012) 139–151.
- [23] F.B. Mostafa, M.A. Samad, M.R. Hossain, Combined effect of viscous dissipation and radiation on unsteady free convective non-Newtonian fluid along a continuously moving vertically stretched surface with no-slip phenomena, Am. J. Comput. Appl. Math. 7 (3) (2017) 71–79.
- [24] A. Hamid, M. Khan, A. Hafeez, Unsteady stagnation-point flow of Williamson fluid generated by stretching/shrinking sheet with Ohmic heating, Int. J. Heat Mass Tran. 126 (2018) 933–940.
- [25] G. Dharmaiah, O.D. Makinde, K.S. Balamurugan, Perturbation analysis of thermophoresis, hall current and heat source on flow dissipative aligned convective flow about an inclined plate, International Journal Thermofluid Science and Technology 7 (1) (2020) 20070103.
- [26] K.V.B. Rajakumar, K.S. Balamurugan, ChV.R. Murthy, M.U. Reddyd, Chemical reaction and viscous dissipation effects on MHD free convective flow past a semi-infinite moving vertical porous plate with radiation absorption, Global J. Pure Appl. Math. 13 (12) (2017) 8297–8322.
- [27] S. Pandikunta, P. Tamalapakula, B.R. Nandanoor, Internal heat generation effect on radiation heat transfer MHD dissipating flow of a micropolar fluid with variable wall heat flux, J. Nav. Architect. Mar. Eng. 15 (1) (2018) 53–64.
- [28] O.J. Fenuga, A.R. Hassan, P.O. Olanrewaju, Effects of radiation and Eckert number on MHD flow with heat transfer rate near a stagnation point over a non-linear vertical stretching sheet, Int. J. Appl. Mech. Eng. 25 (1) (2020) 27–36.
- [29] M. Ferdows, M.D. Shamshuddin, K. Zaimi, Dissipative-radiative micropolar fluid transport in a non-Darcy porous medium with cross-diffusion effects, CFD Lett. 12 (7) (2020) 70–89.
- [30] M. Hasanuzzaman, S. Akter, S. Sharin, M.M. Hossain, A. Miyara, M.A. Hossain, Viscous dissipation effect on unsteady magneto-convective heat-mass transport passing in a vertical porous plate with thermal radiation, Heliyon 9 (3) (2023) e14207.
- [31] P. Cheng, Two-dimensional radiation gas flow by moment method, American Institute of Aeronautics and Astronautics Journal 2 (9) (1964) 1662–1664.
- [32] D.R.V.S.R.K. Sastry, A.S.N. Murti, A double diffusive unsteady MHD convective flow past a flat porous plate moving through a binary mixture with suction or injection, Journal of Fluids 2013 (2013) 935156, https://doi.org/10.1155/2013/935156.
- [33] I.L. Animasaun, Double diffusive unsteady convective micropolar flow past a vertical porous plate moving through binary mixture using modified Boussinesq approximation, Ain Shams Eng. J. 7 (2) (2016) 755–765.
- [34] O.D. Makinde, Free convection flow with thermal radiation and mass transfer past a moving vertical porous plate, Int. Commun. Heat Mass Tran. 32 (10) (2005) 1411–1419.
- [35] G.M.A. Rahman, Effects of MHD on thin films of unsteady micropolar fluid through a porous medium, J. Mod. Phys. 2 (11) (2011) 1290-1304.
- [36] M. Qasim, I. Khan, S. Sheltie, Heat transfer in a micropolar fluid over a stretching sheet with Newtonian heating, PLoS One 8 (4) (2013) e59393.
- [37] L. Talbot, R.K. Cheng, R.W. Schefer, D.R. Willis, Thermophoresis of particles in a heated boundary layer, J. Fluid Mech. 101 (4) (1980) 737–758.
- [38] R. Tsai, Y.P. Chang, T.Y. Lin, Combined effects of thermophoresis and electrophoresis on particle deposition onto a wafer, J. Aerosol Sci. 29 (7) (1998) 811–825.
- [39] G.K. Bachelor, C. Shen, Thermophoresis deposition of particles in gas flowing over cold surfaces, J. Colloid Interface Sci. 107 (1) (1985) 21–37.
- [40] J. Boussinesq, Th'eorie de I, ecoulement tourbillonnant et tumultuex des liquids dans les lits rectilignes a grande section. Gauthier-Villars *Paris*, vol. 1, Open Library OI. 7070543M 1897
- [41] S. Mukhopadhyay, Effects of radiation and variable fluid viscosity on flow and heat transfer along a symmetric wedge, J. Appl. Fluid Mech. 2 (2) (2014) 29–34.
- [42] G.K. Bachelor, An Introduction to Fluid Dynamics, Cambridge University Press, London, 1987.
- [43] I.L. Animasaun, O.O. Anselm, Effects of variable viscosity, Dufour, Soret and thermal conductivity on free convective heat and mass transfer of non-Darcian flow past porous flat surface, Am. J. Comput. Math. 4 (4) (2011) 357–365.
- [44] A. Raptis, Flow of a micropolar fluid past a continuously moving plate by the presence of radiation, International Journal of Heat and Mass Transfer viscoelastic 41 (18) (1998) 2865–2866.
- [45] A. Raptis, Radiation and flow, Int. Commun. Heat Mass Tran. 26 (6) (1999) 889-895.
- [46] M. Ali, M.A. Alim, R. Nasrin, M.S. Alam, Numerical analysis of heat and mass transfer along a stretching wedge surface, J. Nav. Architect. Mar. Eng. 14 (2) (2017) 135–144.
- [47] M. Ali, R. Nasrin, M.A. Alim, Analysis of boundary layer nanofluid flow over a stretching permeable wedge-shaped surface with magnetic effect, J. Nav. Architect. Mar. Eng. 18 (1) (2021) 11–24.
- [48] M.J. Uddin, R. Nasrin, A numerical appraisal of time-dependent magneto-convective thermal-material transfer over a vertical permeable plate, J. Appl. Math. 2023 (2023), 9977857, 19.